Available online at www.sciencedirect.com
SCIENCE DIRECT®
Pergamon
Acta Materialia 51 (2003) 2717–2730
Acta MATERIALIA
www.actamat-journals.com

On the effect of hydrogen on plastic instabilities in metals

Y. Liang [a], P. Sofronis [a,*], N. Aravas [b]

[a] *Department of Theoretical and Applied Mechanics, University of Illinois at Urbana-Champaign, 104 S. Wright Street, Urbana, IL 61801, USA*

[b] *Department of Mechanical and Industrial Engineering, University of Thessaly, Pedion Areos, 38334 Volos, Greece*

Received 23 October 2002; received in revised form 9 January 2003; accepted 4 February 2003

Abstract

Experimental observations and theoretical calculations have demonstrated that hydrogen solute atoms increase the dislocation mobility in metals and alloys, thus promoting highly localized plastic processes which eventually lead to localized ductile rupture. While the underlying mechanism for hydrogen-enhanced dislocation mobility is well understood, little is known on how this mechanism acting at the microscale can lead to macroscopic plastic instability. In this paper, a theoretical investigation is carried out in a specimen under plane-strain tension in an effort to understand how hydrogen-induced softening and lattice dilatation at the microscale can lead to macroscopic i) *shear localization* (*shear banding bifurcation*) or ii) *necking bifurcation*.

Keywords: Hydrogen embrittlement; Dislocation mobility; Shear bands; Necking; Finite element analysis

1. Introduction

It is well known that hydrogen embrittlement is a severe environmental type of failure [1–8]. In a hydrogen environment, materials fail at load levels that are very low compared with those that a hydrogen free material can sustain [9]. Of the many suggestions for an explanation of the hydrogen related failures, the mechanism of hydrogen enhanced localized plasticity (HELP) appears to be a viable one [6,10–14]. The HELP mechanism is based on experimental observations [12–18] and theoretical calculations [19,20] that, in a range of temperatures and strain rates, the presence of hydrogen induces shear localization of the plastic flow [10,14,15,21–29] which results in highly localized ductile rupture process [14,15–18,21–25]. The underlying principle in the HELP mechanism is the shielding of the elastic interactions between dislocations and obstacles by the hydrogen solutes [6,12,19,20], which results in enhanced dislocation mobility [13–15,22,30,31]. A recent and thorough summary of the experimental evidence on hydrogen enhanced dislocation mobility is given in the work by Robertson [32]. While the evidence on the existence and operation of the HELP mechanism is incontrovertible, the detailed mechanism by which enhanced dislocation mobility causes shear localization and fracture in

* Corresponding author. Tel.: +1-217-333-2636; fax: +1-217-244-5707.
E-mail address: sofronis@uiuc.edu (P. Sofronis).

1359-6454/03/$30.00
doi:10.1016/S1359-6454(03)00081-8

bulk specimens remains a subject that is still poorly understood. An attempt to resolve the issue of shear localization in the case of a specimen strained homogeneously in plane-strain has been made recently by Sofronis et al. [33]. It was demonstrated that the presence of hydrogen can indeed induce shear banding bifurcation at macroscopic strains that are about two to three orders of magnitude the initial yield strain of the material.

In the present investigation, the objective is to study the effect of hydrogen on the bifurcation of a homogeneous deformation in a plane-strain tension specimen into a *necking* or a *shear localization* mode of deformation. The plane-strain tension test was chosen for the simplicity it offers in analyzing the conditions leading to plastic instability as it is well known [34,35] that numerical analyses of such phenomena are strongly mesh sensitive and their simulation and identification is harder in a domain with a complex geometry, e.g., the root of a notch tip. In addition, a plane-strain geometry was chosen instead of an axisymmetric one since it is well known [36] that the ductility of the former is less than the ductility of the latter, and this has been demonstrated by the experiments of Clausing [37] on a series of seven structural steels. In accordance, as Rice [38] points out, the plane strain-specimen shows a greater tendency for localization in comparison to the axisymmetric bar specimen. Of course, the analysis presented in this work is easily extended to the axisymmetric bar specimens, and the results are expected to be only quantitatively different.

In a specimen under plane-strain tension, plastic instability can lead to the concentration of plastic flow in a narrow neck [39,40]. The classical theory of Hill [41,42] can be used to study necking as a pure bifurcation problem and such an analysis of necking has been carried out by Cheng et al. [43], Miles [44], Needleman [45], Hutchinson and Miles [46], Burke and Nix [47], Argyris et al. [48], and Petryk and Thermann [49]. The *necking bifurcation* can also be investigated by the introduction of a small initial imperfection (material or geometric) into a homogeneous specimen [50–54]. This way, necking is studied as a pure deformation problem (Chen [55], McMeeking and Rice [56]; Norris et al. [57], Tvergaard et al. [58], Argyris et al. [48], Chen [59], Zbib and Jubran [60], Tvergaard [61], Goldthorpe and Church [62]). Another important type of plastic instability is the bifurcation from homogeneous deformation into a mode whereby the deformation localizes exclusively in a narrow band of intense shear [38,63]. This type of *shear banding bifurcation* or *shear localization* has often been seen around crack tips and in tensile specimens and it is usually a precursor of material failure [38]. Conditions for bifurcation in the form of shear localization have been analyzed in a homogeneous specimen undergoing homogeneous deformation by Rice [38], Rudnicki and Rice [64], and Needleman and Rice [36].

In this work, the role of hydrogen on shear localization will be analyzed first. Next, the critical macroscopic strain for the onset of the necking bifurcation will be sought in the presence of hydrogen either by introducing a geometric imperfection in the shape of the specimen or an initial local perturbation in the stress-free homogeneous hydrogen concentration field. Such a perturbation introduces a local material softening [33] whose magnitude depends directly on the corresponding local hydrogen concentration. This correspondence between a local perturbation and local material softening is predicated on the discussion by Birnbaum and coworkers [7,65] who, summarizing the experimental evidence on HELP, suggested that the flow stress is lower where the hydrogen concentration is higher, and therefore in the region of plastic instability it is reduced relative to the flow stress in the homogeneously deforming volume. In both shear banding and necking bifurcation analyses, the amount of hydrogen in the specimen will be calculated by considering the extent of plastic straining (trapped hydrogen) and hydrostatic stress (hydrogen in normal interstitial lattice sites). Due to the extremely high mobility of the hydrogen solute, the hydrogen populations in trapping sites are assumed to be always in equilibrium with hydrogen in interstitial sites, which is also assumed to be in equilibrium with local hydrostatic stress. The calculated hydrogen concentration is then used to estimate the amount of lattice dilatation [66] and material softening [33] along the lines of the experimental observations on dislocation mobility by Tabata and Birnbaum [21]. Next, a constitutive

law governing the material response in the presence of hydrogen is devised and used to analyze the conditions for shear localization or specimen necking. As will be seen, the calculation of the hydrogen concentrations and the corresponding material softening and dilatation are coupled and therefore, the analysis involves iteration.

2. Hydrogen concentration

Hydrogen is assumed to reside either at normal interstitial lattice sites (NILS) or reversible trapping sites at microstructural defects generated by plastic deformation. The two populations are always in equilibrium according to Oriani's theory [67], such that

$$\frac{\theta_T}{1-\theta_T} = \frac{\theta_L}{1-\theta_L} K_T, \tag{1}$$

where θ_L denotes the occupancy of the interstitial sites, θ_T denotes the occupancy of the trapping sites, $K_T = \exp(W_B/RT)$, W_B is the trap binding energy, R is the gas constant equal to 8.31 J mole^{-1}K^{-1} and T is the absolute temperature. The hydrogen concentration C_T, measured in hydrogen atoms per unit volume, in trapping sites can be phrased as $C_T = \theta_T \alpha N_T$, where α denotes the number of sites per trap, and $N_T = N_T(\varepsilon^p)$ denotes the trap density in number of traps per unit volume as a function of the amount of the local plastic deformation measured in terms of the effective plastic strain ε^p. The hydrogen concentration C_L, measured in hydrogen atoms per unit volume, in interstitial sites can be stated as $C_L = \theta_L \beta N_L$, where β denotes the number of NILS per solvent atom, N_L denotes the number of solvent atoms per unit volume given by $N_L = N_A/V_M$ with $N_A = 6.0232 \times 10^{23}$ atoms per mole being Avogadro's number and V_M the molar volume of the host lattice measured in units of volume per mole.

Hydrogen concentrations C_L in NILS are studied under equilibrium conditions with local stress σ_{ij}. The Fermi-Dirac form [68] is used to calculate the equilibrium hydrogen concentration C_L in terms of the lattice concentration C_0 in the stress-free solid (initial NILS concentration in the absence of any stress, measured in hydrogen atoms per unit volume) as

$$\frac{\theta_L}{1-\theta_L} = \frac{\theta_L^0}{1-\theta_L^0} K_L, \tag{2}$$

where $\theta_L^0 = C_0/\beta N_L$ denotes the initial NILS occupancy, $K_L = \exp(\sigma_{kk} V_H/3RT)$, V_H is the partial molar volume of hydrogen in solution, and the standard summation convention is used over repeated indices throughout.

Combination of Eqs (1) and (2) yields the total hydrogen concentration [33] c, measured in hydrogen atoms per solvent atom, as a function of both the hydrostatic stress and the equivalent plastic strain

$$c = \beta[\theta_L(\sigma_{kk}) + \theta_{TL}(\sigma_{kk}, \varepsilon^p)], \tag{3}$$

where

$$\theta_L(\sigma_{kk}) = \theta_L^0 K_L(\sigma_{kk}) / [(1-\theta_L^0) + \theta_L^0 K_L(\sigma_{kk})] \tag{4}$$

and

$$\theta_{TL}(\sigma_{kk}, \varepsilon^p) = \frac{\alpha N_T(\varepsilon^p)}{\beta N_L} \frac{K_T \theta_L(\sigma_{kk})}{1-\theta_L(\sigma_{kk}) + K_T \theta_L(\sigma_{kk})}. \tag{5}$$

It is mentioned again that in the present treatment there are no transient effects [69,70] in the hydrogen population development. In other words, Eqs (3)–(5) dictate that the total hydrogen concentration at a point is known once the effective plastic strain ε^p and the hydrostatic stress σ_{kk} are known. Of course, as will be discussed in the next section, the values of both the effective plastic strain and hydrostatic stress are dependent on the corresponding amount of hydrogen.

3. Constitutive law

It has been argued by Birnbaum and co-workers [6,7,19,65] that at temperatures and strain rates in which hydrogen embrittlement is experimentally observed hydrogen induces material softening at the microscale by enhancing the dislocation mobility. In a continuum sense, softening can be described through a local flow stress that decreases with increasing hydrogen concentration. It is

emphasized [33] that the term "local flow stress" denotes the intrinsic flow characteristics of a small volume of material at the microscale where hydrogen has concentrated by deformation. "Local flow stress" should not be confused with the flow stress measured "macroscopically", say, in a tensile test. The reason is that while the intrinsic material flow stress decreases with hydrogen [11], the macroscopically measured flow stress may either decrease [10,71–75] or increase with hydrogen [76–79] depending on the degree of hydrogen induced shear localization and the magnitude of the local softening due to the removal of dislocation barriers [6,65]. Thus, from a continuum mechanics perspective, hydrogen-induced material softening can be described through a local flow stress, σ_Y, that decreases with increasing hydrogen concentration [21]. Following Sofronis et al. [33], one may write

$$\sigma_Y(\varepsilon^p,c) = \sigma_0(c)(1 + \varepsilon^p/\varepsilon_0)^N \tag{6}$$

in which, c is the total hydrogen concentration measured in H atoms per solvent atom, $\sigma_0(c)$ is the yield stress in the presence of hydrogen, $\sigma_0 = \sigma_0(0)$ is the yield stress of the material in the absence of hydrogen, and $\varepsilon_0 = \sigma_0/E$ is the corresponding yield strain with E being the Young's modulus. The exponent N is the hardening coefficient which is assumed to remain unaltered by the presence of hydrogen. It is emphasized that the methodology presented in this paper is general and entirely independent of whether N is hydrogen dependent or not. It was chosen that hydrogen does not affect the exponent N in view of the absence of any conclusive experimental evidence. Further, it is assumed that $c < 1$ so that formation of the MH hydride structure (M stands for metal) is avoided in the calculations. A possible suggestion for $\sigma_0(c)$ is a linear form

$$\sigma_0(c) = [(\xi-1)c + 1]\sigma_0, \tag{7}$$

where $\xi \leq 1$ is a softening parameter. Note that when $c = 1$, $\xi = \sigma_0(c)/\sigma_0$ denotes the ratio of the yield stress in the presence of hydrogen to that in the absence of hydrogen at the maximum hydrogen concentration of 1. It should be noted that the proposed model of Eqs (6) and (7) for the hydrogen induced material softening should be viewed only as an attempt to quantify the experimental understanding of the hydrogen effect on dislocation mobility in a continuum sense, and not as reflecting precise material constitutive response.

Formulating the 3-D constitutive equation to describe large strain response in the presence of hydrogen, one starts with the total deformation rate tensor (which is equal to the symmetric part of the velocity gradient) written as $D_{ij} = D^e_{ij} + D^p_{ij} + D^h_{ij}$, where D^e_{ij} is the elastic part, D^p_{ij} is the plastic part, and D^h_{ij} is the part due to the hydrogen-induced lattice distortion. The elastic part of the deformation rate tensor, D^e_{ij}, is modeled as linear and isotropic:

$$D^e_{ij} = \frac{1}{2G}\overset{\nabla}{\sigma'}_{ij} + \frac{1}{9K}\overset{\nabla}{\sigma}_{kk}\delta_{ij}, \tag{8}$$

where the superposed ∇ denotes the Jaumann or co-rotational rate which exhibits proper material invariance for rigid rotation, $\sigma'_{ij} = \sigma_{ij} - \sigma_{kk}\delta_{ij}/3$ is the deviatoric stress, δ_{ij} is the Kronecker delta, and G and K are the elastic shear and bulk moduli, respectively.

The hydrogen-induced deformation rate D^h_{ij} is purely dilatational [66] and can be stated as

$$D^h_{ij} = \frac{d}{dt}\left[\ln\left(1 + \frac{(c-c_0^{tot})}{3}\lambda\right)\right]\delta_{ij}, \tag{9}$$

where d/dt denotes material time differentiation, $c_0^{tot} = \beta[\theta_L(0) + \theta_{TL}(0,0)]$ is the initial hydrogen concentration in NILS and the traps before the application of stress and plastic straining (see Eq. (3)), $\lambda = \Delta v/\Omega$ is the normalized lattice dilatation per hydrogen atom introduced into solution, $\Delta v = V_H/N_A$ is the volume increase per hydrogen atom, and Ω is the mean atomic volume of the host metal atom. Eq. (9) essentially denotes that the normalized stretching of an infinitesimal material fiber is equal to one third of the experimentally observed normalized dilatation. Notice that in the case of infinitesimal deformations, that is, when c is not very different from c_0^{tot}, Eq. (9) reduces to the usual form of an infinitesimal strain rate, $\dot{\varepsilon}^h_{ij} = (\dot{c}\Delta v/3\Omega)\delta_{ij}$.

For the plastic response, the material is assumed to be rate-independent, yield according to the von Mises criterion, and harden isotropically during plastic straining. Then the associated flow rule is given by [33]

$$D^p_{ij} = \frac{1}{\partial\sigma_Y/\partial\varepsilon^p}\left(\frac{3\sigma'_{kl}}{2\sigma_e}\overset{\nabla}{\sigma}_{kl} - \frac{\partial\sigma_Y}{\partial c}\dot{c}\right)\frac{3\sigma'_{ij}}{2\sigma_e}, \tag{10}$$

where $\sigma_e = \sqrt{3\sigma'_{ij}\sigma'_{ij}/2}$ is the Mises equivalent stress. From Eq. (10) one observes that as the local hydrogen concentration in the material changes, so does the plastic strain. Substitution of Eqs (8), (9) and (10) into $D_{ij} = D^e_{ij} + D^p_{ij} + D^h_{ij}$ gives the constitutive law for the elastoplastic material response in the presence of hydrogen as

$$\overset{\nabla}{\sigma}_{ij} = L_{ijkl}D_{kl}, \tag{11}$$

where

$$L_{ijkl} = 2G\left\{\frac{1}{2}(\delta_{ik}\delta_{jl} + \delta_{il}\delta_{jk}) - \left[\left(\frac{1}{3}A_2 - \frac{1}{6G}\right)\delta_{ij} + \frac{3A_1}{2\sigma_e^2}\sigma'_{ij}\right]\frac{B_2\sigma'_{kl} - B_1\delta_{kl}}{A_1B_2 - A_2B_1} - \left[\frac{1}{3}B_2\delta_{ij} + \frac{9}{4h'\sigma_e^2}\sigma'_{ij}\right]\frac{A_2\sigma'_{kl} - A_1\delta_{kl}}{A_2B_1 - A_1B_2}\right\} \tag{12}$$

and

$$A_1 = \frac{\mu\sigma_e}{h'},\quad A_2 = \frac{1}{3K} + \Lambda(c)\frac{\partial c}{\partial\sigma_{pp}} + \frac{\mu}{h'}\Lambda(c)\frac{\partial c}{\partial\varepsilon^p},$$

$$B_1 = \frac{1}{2G} + \frac{3}{2h'},\quad B_2 = \frac{1}{h'}\frac{3}{2\sigma_e}\Lambda(c)\frac{\partial c}{\partial\varepsilon^p},$$

$$\Lambda(c) = \frac{\lambda}{1 + \lambda(c - c_0)/3},$$

$$h' = \frac{\partial\sigma_Y}{\partial\varepsilon^p} + \frac{\partial\sigma_Y}{\partial c}\frac{\partial c}{\partial\varepsilon^p},\quad \mu = -\frac{\partial\sigma_Y}{\partial c}\frac{\partial c}{\partial\sigma_{kk}}. \tag{13}$$

Notice that h' is the plastic tangent modulus that accounts for the hydrogen effect on the flow stress. The parameter B_2 is a plastic dilatancy factor which is similar to the dilatancy factor β [33] in the model of Rudnicki and Rice [64] for porous infiltrated geomaterials which are plastically compressible, and the parameter μ denotes the corresponding pressure sensitivity of yield. The parameter $\Lambda(c)$ provides the hydrogen-induced material dilatation rate (see Eq. (9)) and the parameter A_2 is a measure of how the elastic material compressibility is affected by the presence of hydrogen.

4. Hydrogen-induced shear localization

As has been discussed in the introduction, shear localization is a form of plastic instability whereby the deformation localizes into a narrow band of intense shear. In this section the onset of such an instability in a homogeneous deformation field is studied in relation to the nature of the constitutive moduli which change during loading by the presence of hydrogen such that the equations governing incremental equilibrium lose their ellipticity [63]. In other words, at the state of loading at which a critical change in the constitutive moduli L of Eq. (11) is impending, an additional increment of load is accommodated not by continued homogeneous deformation but by a localized deformation in a band of intense shear instead. As Rice [38] points out, the bifurcation from a homogeneous plastic flow into a mode of shear localization is a limiting form of plastic instability in the sense that other forms of instability such as necking or shear localization from an initial material or geometric inhomogeneity may proceed it. For a homogeneous solid, the condition for bifurcation of the homogeneous deformation into a mode of intense shear banding is stated as [36,38]

$$\det[n_kL_{kijl}n_l + A_{ij}] = 0, \tag{14}$$

where **n** is the unit vector normal to the direction of the forming shear band in the current configuration (see inset of Fig. 3), and $A_{ij} = (-\sigma_{ij} + \sigma_{ik}n_kn_j + \sigma_{kl}n_kn_l\delta_{ij} - \sigma_{mj}n_in_m)/2$. Following Rudnicki and Rice [64], one can recast the condition (14) for shear localization in the presence of hydrogen into one in which the hardening modulus $h = h'/3 = [\partial\sigma_e/\partial\varepsilon^p + (\partial\sigma_e/\partial c)(\partial c/\partial\varepsilon^p)]/3$ reduces upon loading to a critical value h_{cr} which depends on the current state of stress, hydrogen concentration, and material constants [33,64,80].

Condition (14) for shear localization was checked in the case of a niobium specimen undergoing homogeneous tension in plane strain. Niobium was chosen as data are readily available. The specimen, shown in Fig. 1, was loaded by displacement increments Δu_2 in the x_2 direction, constrained in the x_3 direction, i.e. $u_3 = 0$ at any point, and its sides normal to the x_1 axis were traction free. Before straining the specimen was assumed to

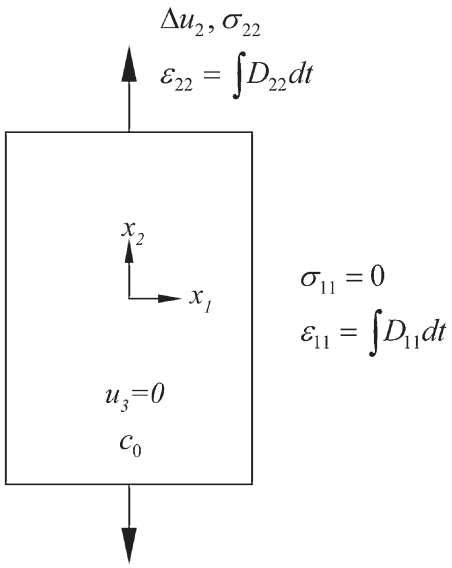

Fig. 1. A specimen strained homogeneously in plane strain by displacement increments Δu_2 in the x_2 direction. Before straining, the specimen is at a uniform initial concentration c_0 (H/M) at normal interstitial lattice sites (NILS).

be stress free and at a uniform NILS concentration $c_0 = \beta\theta_L(0)$ measured in H atoms per solvent atom (H/M). Upon straining, uniform redistribution of the hydrogen solutes occurs so that hydrogen is always in local equilibrium with the local stress and strain as dictated by Eq. (3). Since hydrogen is assumed to be provided by a chemical reservoir, an arrangement corresponding to "far field concentration" kept constant at c_0, the present calculation corresponds to a constant chemical potential for the hydrogen solute. At the end of each loading increment, the stresses and strains in the specimen are known (for the calculation details, please see the appendix in reference [33]) and the condition for shear localization is checked for every possible orientation of the unit vector **n** (see inset of Fig. 3). Straining of the specimen continued until condition (14) was satisfied, and the macroscopic logarithmic strain ε_{22} at this point was identified as the critical strain ε_{22}^b for the onset of shear localization. The procedure was repeated for different values of the initial hydrogen concentration c_0.

In the calculations, the hydrogen trap sites were associated with dislocations in the deforming metal [81]. Assuming one trap site per atomic plane threaded by a dislocation [81–83], one finds that the trap site density in traps per cubic meter is given by $N_T = \sqrt{2}\rho/a$, where ρ is the dislocation density and a is the lattice parameter. The dislocation density ρ measured in dislocation line length per cubic meter was considered to vary linearly with the effective plastic strain ε^p [84], i.e., $\rho = \rho_0 + \gamma\varepsilon^p$ for $\varepsilon^p \leq 0.5$ and $\rho = 10^{16} + \rho_0$ for $\varepsilon^p > 0.5$, where $\rho_0 = 10^{10}$ line length/m^3 denotes the dislocation density for the annealed material and $\gamma = 2.0 \times 10^{16}$ line length/m^3. The parameter α was taken equal to 1 (one trapping site per trap), the parameter β was set equal to 1 and this corresponds to a maximum NILS concentration of 1 hydrogen atom per solvent lattice atom. Hydrogen was assumed to expand the lattice isotropically and its partial molar volume in solution was $V_H = 1.88$ cm^3/mole which corresponds to $\lambda = 0.174$. The molar volume of niobium was 10.852×10^{-6} m^3/mole which implies that the number of the available NILS was $N_L = 5.55 \times 10^{28}$ solvent lattice atoms per m^3. The lattice parameter was $a = 3.3 \times 10^{-10}$m, the Poisson's ratio $\nu = 0.34$, Young's modulus $E = 115$ GPa, the yield stress in the absence of hydrogen $\sigma_0 = 400$ MPa, the hardening coefficient $N = 0.1$, and the softening parameter ξ was set equal to 0.1. The trap binding energy was taken equal to $W_B = 29.2$ kJ/mole [85] and the temperature of the system was 300 K.

Fig. 2 shows the normalized effective Mises stress σ_e/σ_0 ($\sigma_e = \sqrt{\sigma_{22}^2 + \sigma_{33}^2 - \sigma_{22}\sigma_{33}}$) plotted against the effective plastic strain ε^p at various initial hydrogen concentrations c_0. Clearly, the material becomes increasingly softer with decreasing tangent modulus as c_0 increases. As discussed by Rudnicki and Rice [64], a lower tangent modulus is associated with lower values of the macroscopic loads at which shear banding bifurcation is triggered. The critical applied macroscopic strain $\varepsilon_{22}^b/\varepsilon_0$ at which shear localization commences is shown plotted against the initial hydrogen concentration c_0 in Fig. 3. Fig. 4 shows the result of the calculation of h and h_{cr} as a function of the macroscopic strain for three initial hydrogen concentrations $c_0 = 0.1$, 0.3, and 0.5 H/M. The points where the two curves intersect indicate the level of the macroscopic strain, ε_{22}^b, at which shear localization occurs. The critical hardening modulus h_{cr}

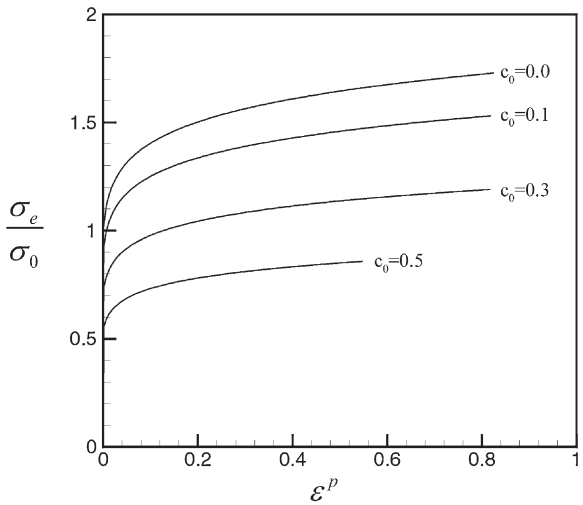

Fig. 2. Normalized effective Mises stress σ_e/σ_0 versus effective plastic strain ε^p at various initial hydrogen concentrations c_0 (H/M). The hardening exponent is $N = 0.1$, the softening parameter $\xi = 0.1$ (see Eq. (7)), and σ_0 is the yield stress in the absence of hydrogen.

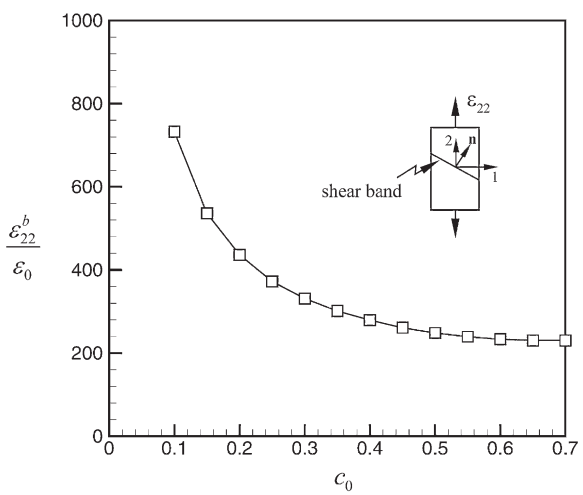

Fig. 3. Critical normalized macroscopic strain $\varepsilon_{22}^b/\varepsilon_0$ at the onset of shear localization at various initial hydrogen concentrations c_0, $N = 0.1$, and $\xi = 0.1$. The parameter $\varepsilon_0 = \sigma_0/E$ is the yield strain in uniaxial tension in the absence of hydrogen.

increases rapidly with strain and assumes a positive value. At low initial hydrogen concentrations, the hydrogen-induced softening effect is mild and this is demonstrated in a correspondingly small hydrogen-induced reduction of the tangent modulus h of

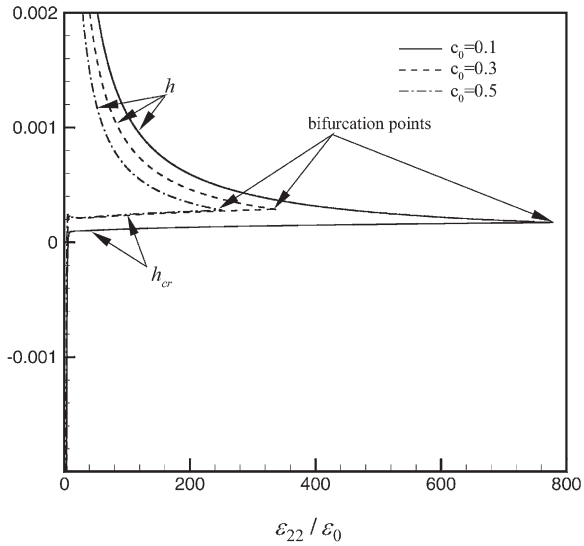

Fig. 4. Plot of the tangent modulus h and the critical tangent modulus h_{cr} against the normalized applied macroscopic strain $\varepsilon_{22}/\varepsilon_0$ at various initial hydrogen concentrations c_0 (H/M), $N = 0.1$, and $\xi = 0.1$. Shear localization occurs when $h = h_{cr}$.

the material. As a result, the intersection between the h and h_{cr} curves (see Fig. 4) occurs at large strains, that is, shear localization requires a large macroscopic strain at small initial hydrogen concentrations. On the other hand, at larger initial hydrogen concentrations the softening effect on the hardening modulus becomes more pronounced and therefore, it takes less strain for the condition $h = h_{cr}$ to be met.

It is known that shear banding bifurcation can never take place in a hydrogen-free power law hardening ($h > 0$) Mises material under plane-strain tension since $h_{cr} < 0$ [64]. However, the present study demonstrates that hydrogen-induced material softening and lattice dilatation at the microscale can indeed induce shear localization at the macroscale despite the fact that the material continues to exhibit positive hardening in the presence of hydrogen (Fig. 2). Thus one may describe the hydrogen effect as causing the critical modulus h_{cr} for shear banding bifurcation to be positive and increase with initial hydrogen concentration c_0. It should be noted that in the present study, shear localization happens at a macroscopic elongation of the specimen greater than 150%, which is exceedingly large in comparison to the experimen-

tally observed shear banding at strains very close to the initial yield [86]. This overestimation of the critical localization strain might be attributed to the J_2 flow theory used in the present analysis, as is well known that this theory is characterized by a stiff response to plastic flow [35]. Other theories such as the one with von Mises yielding and a vertex on the yield surface are known to be more sensitive to shear localization [38,64]. The study of this subject is presented in a subsequent publication.

5. The hydrogen effect on necking instability

To simulate the onset of necking in plane-strain tension, it is customary to carry out finite element simulations on specimens that feature either an initial small geometric imperfection or a small material inhomogeneity [50–54]. The idea is that the level of applied macroscopic strain at which elastic unloading commences at some material point in the specimen is very close to the strain at which necking bifurcation is triggered in the "perfect" specimen. It should be remembered that necking bifurcation in a cylinder strained by displacement control in uniaxial tension usually commences after the macroscopically applied load attains its maximum value [39,45,46].

Consider a stress-free specimen of half-length l with a small geometric imperfection shown greatly exaggerated in Fig. 5(a) only in the first quadrant due to symmetry. The specimen is at a uniform initial hydrogen concentration c_0 throughout. The half-width of the specimen over $0 \le x_2 \le l/6$ is constant and equal to 0.9999 the half-width w at $x_2 = l$, varies linearly over $l/6 \le x_2 \le l/3$, and is constant and equal to w over $l/3 \le x_2 \le l$. Also, consider a stress-free specimen of the same dimensions but with no geometric imperfection (Fig. 5(b)), with a

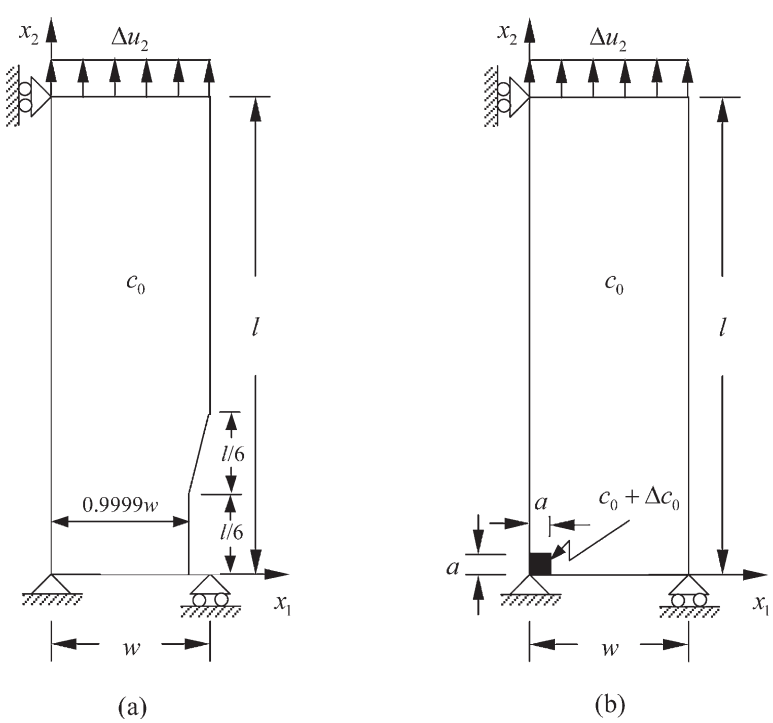

Fig. 5. The first quadrant of two specimens strained in plane strain by displacement increments in the x_2 direction. The half-width of the specimens is $w = l/3$. (a) Specimen with a geometric imperfection which before straining is at a uniform hydrogen concentration c_0 throughout; (b) Specimen which before straining is at an initial concentration $c_0 + \Delta c_0$ in a small region of size $a = l/30$ and a concentration c_0 in the rest of the domain. The parameter Δc_0 denotes a small concentration perturbation.

uniform initial hydrogen concentration c_0 throughout except at a square region at the center of the specimen in which the initial hydrogen concentration is $c_0 + \Delta c_0$, where Δc_0 is a small perturbation. The size of the perturbation region is assumed to be $a = l/30$. Loading of both specimens of Fig. 5 was carried out incrementally by displacement increments Δu_2 at $x_2 = l$ under plane strain conditions. The problem formulation and the related material parameters are exactly the same as in Section 4. However, owing to the initial geometric imperfection (Fig. 5(a)) and initial concentration perturbation (Fig. 5(b)), both the hydrogen and deformation fields develop inhomogeneously during straining. The solutions to the coupled problem for the hydrogen concentration field and the large-strain elastoplastic boundary value problem were obtained by using the general purpose finite element program ABAQUS with a "user subroutine" (UMAT) incorporating the material model described by Eqs (3) and (11). The mesh layouts used in the calculations consisted of 10 (or 20) element sides along the x_1-axis and 30 (or 60) element sides along the x_2-axis (Fig. 5).

Figs 6 and 7 show the normalized average applied macroscopic stress σ_{22}/σ_0 and applied force $F_2/(2\sigma_0 w)$ in the x_2-direction plotted against the normalized average macroscopic logarithmic strain $\varepsilon_{22}/\varepsilon_0$ for an initial hydrogen concentration $c_0 = 0.3$ H/M. The macroscopic strain ε_{22} was calculated through $\varepsilon_{22} = \ln(1 + u_2/l)$ and the macroscopic stress σ_{22} through $\sigma_{22} = F_2/2(w + u_1(x_1 = w, x_2 = l))$. In the homogeneous solution (i.e. for a perfect specimen with no initial imperfection or hydrogen concentration perturbation), it can be seen that the macroscopic stress σ_{22}/σ_0 increases monotonically with increasing strain even though hydrogen decreases the rate of hardening with increasing plastic straining. At the same time, the applied force decreases gradually after attaining a maximum at $\varepsilon_{22} = 28.4\varepsilon_0$ for all three cases, namely homogeneous, with geometric imperfection, and initial hydrogen perturbation. For the non-homogeneous cases, the response of the specimen is identical with the homogeneous response for straining up to a certain strain (see Figs 6 and 7) which is slightly larger than $\varepsilon_{22} = 28.4\varepsilon_0$. As straining continues, the applied force begins to deviate

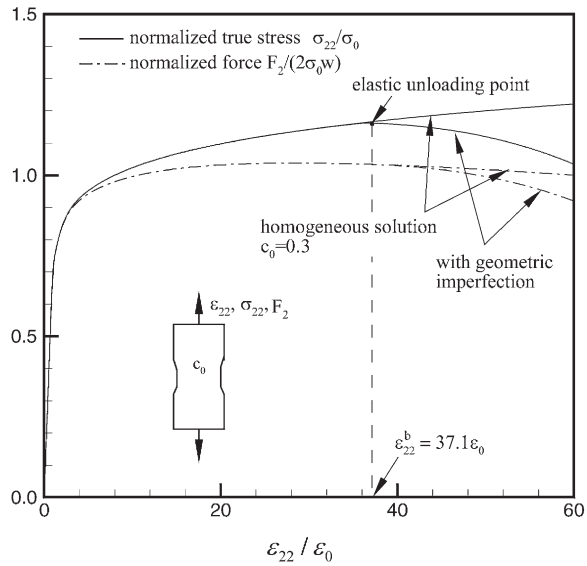

Fig. 6. Plot of normalized macroscopic stress σ_{22}/σ_0 and applied force $F_2/(2\sigma_0 w)$ versus normalized macroscopic strain $\varepsilon_{22}/\varepsilon_0$ for the homogeneous solution (case of specimen with no geometric imperfection or initial hydrogen perturbation) and the solution for the specimen with a geometric imperfection (Fig. 5(a)) at an initial hydrogen concentration $c_0 = 0.3$ H/M for both solutions. The hardening exponent was $N = 0.1$ and $\xi = 0.1$.

from that for the homogeneous case and at a certain strain slightly larger than the deviation strain, elastic unloading is observed to occur at $x_1 = 0, x_2 = l$. In addition, the force drops at a faster rate than that in the homogeneous case; and unlike the homogeneous case, the macroscopic stress σ_{22}/σ_0 begins to decrease with strain monotonically. The macroscopic strain ε_{22}^b at which elastic unloading first occurs in the non-homogeneous specimens is considered to be a good estimate of the strain at which the deformation of the homogeneous (perfect) specimen bifurcates and follows the secondary bifurcation branch which eventually leads to necking (the primary branch is continued deformation characterized by uniform reduction of the cross section throughout the length of the specimen).

The development of the necking event in the case of the specimen with the initial hydrogen concentration perturbation is shown in the contour plots of Fig. 8 in which the distribution of the normalized effective plastic strain $\varepsilon^p/\varepsilon_r^p$ is plotted as

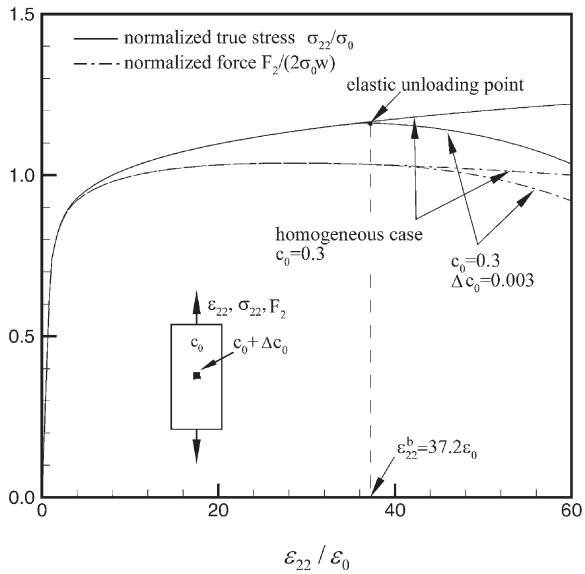

Fig. 7. Plot of normalized macroscopic stress σ_{22}/σ_0 and applied force $F_2/(2\sigma_0 w)$ versus normalized macroscopic strain $\varepsilon_{22}/\varepsilon_0$ for the homogeneous solution (case of specimen with no geometric imperfection or initial hydrogen perturbation) and the solution for the specimen with an initial hydrogen perturbation (Fig. 5(b)) at an initial hydrogen concentration c_0 = 0.3 H/M for both solutions. The perturbation is $\Delta c_0/c_0$ = 0.01.

a function of the normalized macroscopic strain $\varepsilon_{22}/\varepsilon_0$, where ε_r^p is the uniform remote effective plastic strain at $x_2 = l$. Almost upon loading ($\varepsilon_{22}/\varepsilon_0$ = 5.03), two narrow bands with higher deformation intensity are forming at the center of the specimen (Fig. 8(a)). As straining proceeds, the deformation of the specimen concentrates in these two bands (Fig. 8(b)) which propagate at higher and higher intensities toward the sides of the specimen (Fig. 8(c)). At the same time the deformation in the rest of the solid, ε_r^p, continues to increase. It should be noted that at these stages of loading the specimen is still rectangular and no macroscopic instability (bifurcation from the homogeneous solution) has occured. At $\varepsilon_{22}/\varepsilon_0$ = 43.74, the two bands have clearly ceased to be the dominant pattern of deformation, the deformation is widespread all over the central part of the specimen, while elastic unloading begins to take place at the remote parts of the specimen. A markedly distinct feature of the deformed solid is that its shape now is no longer rectangular and the cross-sectional area at

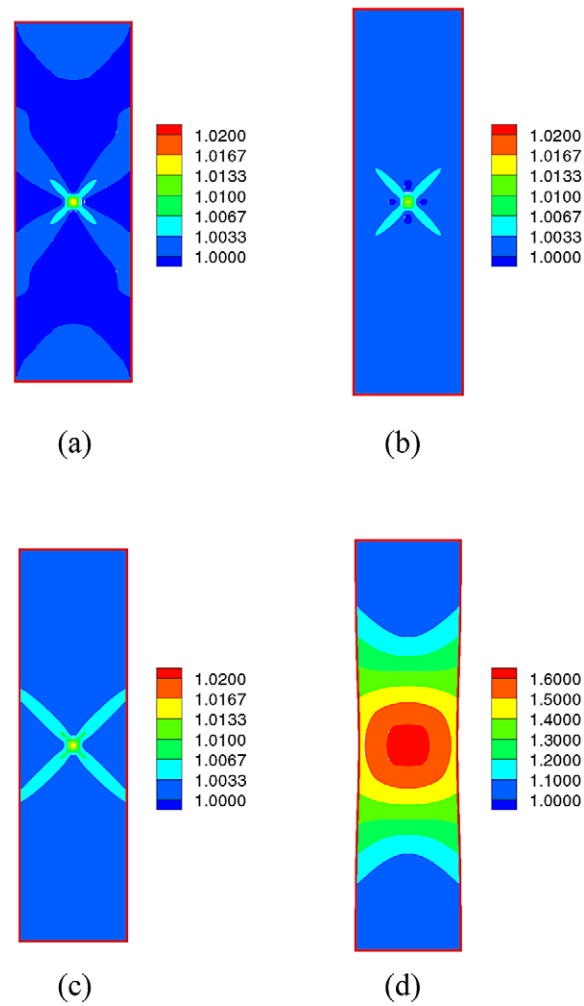

Fig. 8. Contours of the normalized effective plastic strain $\varepsilon^p/\varepsilon_r^p$ for the specimen with an initial hydrogen perturbation Δc_0 = 0.003 H/M over c_0 = 0.3 H/M at (a) $\varepsilon_{22}/\varepsilon_0$ = 5.03 and ε_r^p = 0.0140; (b) $\varepsilon_{22}/\varepsilon_0$ = 25.04 and ε_r^p = 0.09298; (c) $\varepsilon_{22}/\varepsilon_0$ = 29.40 and ε_r^p = 0.1103; (d) $\varepsilon_{22}/\varepsilon_0$ = 42.92 and ε_r^p = 0.1345. The parameter ε_r^p is the remote plastic strain at $x_2 = l$.

the center is smaller than any other in the rest of the specimen.

In Fig. 9 the normalized necking bifurcation strain $\varepsilon_{22}^b/\varepsilon_0$ is plotted against the initial hydrogen concentration c_0. Clearly the two specimens (Fig. 5(a) with the geometric imperfection and Fig. 5(b) with the initial hydrogen concentration perturbation) used to identify the bifurcation strain in the homogeneous solution lead to slightly differ-

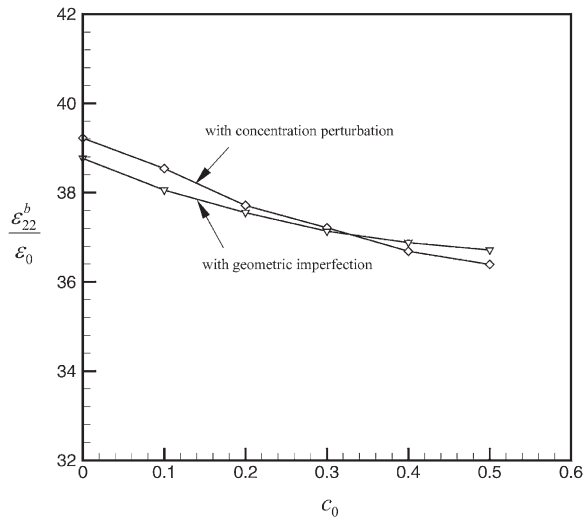

Fig. 9. Normalized necking bifurcation strain $\varepsilon_{22}^b/\varepsilon_0$ as a function of the initial hydrogen concentration c_0 for the two specimens, i.e., the one with geometric imperfection and the one with hydrogen concentration perturbation. For the calculations with concentration perturbation, the magnitude of the perturbation was $\Delta c_0/c_0 = 0.01$ for $c_0 > 0.0$ and $\Delta c_0 = 0.0001$ for $c_0 = 0.0$.

ent estimates. However, this is an expected result as the corresponding boundary value problems associated with the two specimens are different. This is the case even when $c_0 = 0$ throughout the specimen; while the specimen of Fig. 5(a) is completely hydrogen-free, the specimen of Fig. 5(b) has its perturbation region at $\Delta c_0 = 0.0001$ H/M. Fig. 9 demonstrates that the bifurcation strain decreases as the initial uniform hydrogen concentration increases. This is analogous to the fact that the critical strain at which shear localization occurs in a homogeneously strained body has been found to decrease with increasing initial hydrogen concentration (see Fig. 3). Therefore one may infer from this figure that hydrogen reduces the macroscopic strain at which the necking bifurcation takes place.

6. Discussion

A constitutive model based on classical J_2-flow theory for the elastoplastic material response in the presence of hydrogen has been presented for the case of hydrogen being in equilibrium with local stress. The model is based on experimentally verified hydrogen effects, namely lattice dilatation and material softening resulting from hydrogen-enhanced dislocation mobility at the microscale.

The results show that hydrogen can trigger shear localization of the plastic deformation in a specimen under plane-strain tension. It is emphasized that the predicted shear localization is a result of the hydrogen effect on the constitutive law and that such shear banding bifurcation is not possible in the absence of hydrogen for a specimen that work-hardens. However, the values of the macroscopic load at which this constitutively-driven bifurcation takes place are exceedingly high as shear localization has been observed at macroscopic strains estimated to be a few times larger than the initial yield strain ε_0 [86]. Two specimens, one with a geometric imperfection and another with an initial hydrogen concentration perturbation were used to estimate the necking bifurcation strain in a homogeneous specimen strained under plane-strain conditions. An important conclusion drawn from the simulation results is that hydrogen reduces the strain at which necking bifurcation commences.

Looking at the deformation patterns shown in Fig. 8, one can state that the process responsible for the onset of the necking instability, i.e. the band formation, started immediately upon loading the specimen. Generalizing, one may argue that the establishment of a criterion on the load bearing capacity of a structure in the presence of hydrogen might be sought in identifying a critical time or load level at which a shearing event triggered from a material inhomogeneity (internal or at the surface of a specimen) takes up a critical size. Finite element simulations of hydrogen-assisted local plastic deformation at the notch root of a four-point bend specimen are presently carried out. The goal is to detect whether the presence of the notch accelerates the propagation of the shear bands that form at the basis of the notch due to the local material softening resulting from the inhomogeneous distribution of hydrogen at the notch root. Such acceleration of the shear bands may promote a faster formation of the plastic hinge that leads to the loss of the load bearing capacity.

The discussion in the previous paragraph is

predicated on the fact that microstructural material defects such as grain boundaries, dislocations, precipitates, internal material interfaces are known to trap hydrogen at amounts larger than the NILS can accommodate. Such trapping of hydrogen in conjunction with the raising of the stress and plastic flow around the defects may lead to intense local hydrogen accumulations. As a result, the associated local flow stress and dilatation inhomogeneities can lead to local shear band formation around the defects which in turn may be responsible for changes in the overall behavior of a solid. Indeed, in the case of nickel in which the trap binding energy for hydrogen to the grain boundary is 11.6 kj/mole [87], Lassila and Birnbaum [87] estimated that at 253 K there is a layer which extends about 35 nm from the grain boundaries in which the hydrogen concentration is 230 times larger than the concentration in the bulk of the grain when the fracture appears 100% "intergranular". Carrying high resolution TEM studies of these "intergranular" fractures, Lassila and Birnbaum [88,89] concluded that this "intergranular" fracture occurs by highly localized ductile process [25,31] in which the flow stress in the vicinity of the grain boundaries is reduced by the high hydrogen concentrations.

In the present work, the numerical simulation results were derived on the basis of a continuum constitutive model in which yield is sensitive to pressure and the overall dilatation has a plastic component. It is well known that the response of materials to necking and shear localization is strongly dependent on the continuum model used to describe their constitutive behavior [38,62,64]. On the other hand, laboratory specimens never deform uniformly under tension. Plastic deformation always takes place by slip along slip lines and shear bands. Thus as soon as slip initiates, hydrogen at the slip lines or bands increases due to hydrogen diffusion to the dislocations. As the concentration of hydrogen increases locally, the material softens locally and shear localization is enhanced. Obviously to account for these types of behavior a dislocation-based model of the material response should be adopted (e.g. Zerilli and Armstrong [90] and Bammann [91]). The hydrogen effects on dislocation spacing [6,7,19] and strength of obstacles [6,7] to dislocation motion are definitely two important microstructural ingredients that such a model should address. With regard to the strain rate sensitivity of the material, it should be borne in mind that hydrogen embrittlement is a phenomenon that takes places at very low strain rates (in general, $\leq 10^{-5}$) as Birnbaum and Sofronis [6] discuss. Hence, it is not expected that strain rate at such low levels has a significant impact on either necking or shear localization. Moreover, it is well known that in the absence of hydrogen, very small amounts of strain-rate dependence can significantly retard the onset of necking [62,92–96] and shear localization [94,97–99] at realistic stresses, as bifurcation in viscoplastic materials is controlled by the elastic stiffness. In view of this discussion, the continuum model devised in the present work can be viewed as an idealized model that provides an upper bound value for the strains at which necking and shear localization commence.

7. Conclusion

It has been demonstrated on the basis of the J_2-flow constitutive theory properly modified to account for experimentally observed hydrogen effects on material behavior that hydrogen reduces the macroscopic strain at which necking bifurcation commences in a specimen under plane-strain tension. Further, simulations indicate that hydrogen induces shear banding bifurcation which is not possible in a hydrogen-free work hardening material under plane-strain tension. A local hydrogen inhomogeneity has been shown to trigger local shear band formation that promotes necking instability. Therefore, on the basis of the present constitutive model one may argue that hydrogen i) intensifies and accelerates the deformation modes that take place in a hydrogen free material; ii) can lead to localized shear band formation. Improvement on the predicted values of load for necking and shear localization requires a dislocation-mechanics model for the description of the material constitutive response.

Acknowledgements

Financial support for this research was provided by NASA through grant NAG 8-1751. Additional support from the International Program of the College of Engineering of the University of Illinois at Urbana-Champaign, directed by Prof. Carl Altstetter, which facilitated collaboration between the authors at the University of Illinois and the University of Thessaly is gratefully acknowledged.

References

[1] Gerberich WW, Chen YT. Metall Trans A 1975;6:271.
[2] Thompson AW, Bernstein IM. In: Staehle RW, Fontana M, editors. Advances of corrosion science and technology, Vol. 7. 1980. p. 83.
[3] Hirth JP. Metall Trans A 1980;11:861.
[4] Chen SH, Katz Y, Gerberich WW. Phil Mag 1991;63:131.
[5] Chen X, Gerberich WW. Metall Trans A 1999;22:59–70.
[6] Birnbaum HK, Sofronis P. Mater Sci Eng A 1994;176:191.
[7] Birnbaum HK, Robertson IM, Sofronis P, Teter D. In: Magnin T, editor. Corrosion deformation interactions CDI'96 (Second International Conference, Nice, France, 1996). Great Britain: The Institute of Materials; 1997. p. 172.
[8] McMahon Jr. CJ. Eng Fracture Mechanics 2001;68:773.
[9] Symons D. Metall Trans A 1998;29:1265.
[10] Beachem CD. Metall Trans 1972;3:437.
[11] Meyers SM et al. Rev Mod Phys 1992;64:559.
[12] Sirois E, Birnbaum HK. Acta Metall 1992;40:1377.
[13] Shih D, Robertson IM, Birnbaum HK. Acta Metall 1988;36:111.
[14] Robterson IM, Birnbaum HK. Acta Metall 1986;34:353.
[15] Tabata T, Birnbaum HK. Scr Metall 1984;18:231.
[16] Lynch SP. Acta Metall 1988;36:2639.
[17] Lynch SP. Metallography 1989;23:147.
[18] Lynch SP. In: Magnin T, editor. Corrosion deformation interactions CDI'96 (Second International Conference, Nice, France, 1996). Great Britain: The Institute of Materials; 1997. p. 206.
[19] Sofronis P, Birnbaum HK. J Mech Phys Solids 1995;43:49.
[20] Sofronis P. J Mech Phys. Solids 1995;1385:43.
[21] Tabata T, Birnbaum HK. Scr Metall 1983;17:947.
[22] Bond GM, Robertson IM, Birnbaum HK. Acta Metall 1987;35:2289.
[23] Bond GM, Robertson IM, Birnbaum HK. Acta Metall 1988;36:2193.
[24] Rozenak P, Robertson IM, Birnbaum HK. Acta Metall 1990;38:2031.
[25] Eastman J, Matsumoto T, Narita N, Heubaum N, Birnbaum HK. In: Bernstein IM, Thompson AW, editors. Hydrogen in metals. New York: Metallurgical Society of AIME; 1981. p. 397.
[26] Lee TD, Goldenberg T, Hirth JP. Metall Trans A 1979;10:199–208.
[27] Lee TD, Goldenberg T, Hirth JP. Fracture 1977, Vol. 2. Waterloo: University of Waterloo Press, 1977 pp. 243.
[28] Onyewenyi OA, Hirth JP. Metall Trans A 1983;14:259.
[29] Onyewenyi OA. In: Oriani RA, Hirth JP, Smialowski M, editors. Hydrogen degradation of ferrous alloys. New Jersey: Noyes Publications; 1985. p. 414.
[30] Robertson IM, Birnbaum HK. Scr Metall 1984;18:269.
[31] Matsumoto T, Eastman J, Birnbaum HK. Scr Metall 1981;15:1033.
[32] Robertson IM. Eng Fracture Mechanics 2001;68:671.
[33] Sofronis P, Liang Y, Aravas N. Eur J Mech A-Solids 2001;20:857.
[34] Ortiz M, Leroy Y, Needleman A. Com Meth Appl Mech Eng 1987;61:189.
[35] Needleman A, Tvergaard V. In: Oden TJ, Carey GF, editors. Finite elements-special problems of solid mechanics, Vol. V. Englewood Cliffs, NJ: Prentice Hall; 1984. p. 94.
[36] Needleman A, Rice JR. In: Koistinen DP, Wang N-M, editors. Mechanics of sheet metal forming. New York: Plenum Press; 1978. p. 237.
[37] Clausing DP. Int J Fracture Mech 1970;6:71.
[38] Rice JR. Title. In: Koiter WT, editor. Proceedings of the 14th International Congress on Theoretical and Applied Mechanics. North-Holland Publishing Corporation; 1976. p. 207.
[39] Cottrell A. An introduction to metallurgy, 2nd ed. The Institute of Materials, Cambridge University Press, 1975.
[40] Tvergaard V. J Appl Mech 1999;66:3.
[41] Hill R. J Mech Phys Solids 1958;6:236.
[42] Hill R. In: Lavrentiev MA, editor. Problems of continuum mechanics. Philadelphia, PA: Society for Industrial and Applied Mathematics; 1961. p. 155.
[43] Cheng SY, Ariaratnam ST, Dubey RN. Q Appl Math 1971;29:41.
[44] Miles JP. J Mech Phys Solids 1971;19:89.
[45] Needleman A. J Mech Phys Solids 1972;20:111.
[46] Hutchinson JW, Miles JW. J Mech Phys Solids 1974;22:61.
[47] Burke MA, Nix WD. Int J Solids Structures 1979;15:379.
[48] Argyris JH, Doltsinis J, St. Pimenta PM, Wustenberg H. Com Meth Appl Mech Eng 1982;32:3.
[49] Petryk H, Thermann K. Int J Solids Structures 1992;29:745.
[50] Hutchinson JW. Title. In: Yih C-S, editor. Adv Appl Mech, Vol. 14. Academic Press; 1974. p. 67.
[51] Tvergaard V. Int J Solids Structures 1977;13:957.
[52] Tvergaard V. ZAMM 1980;60:T26.
[53] Tomita Y, Shindo A, Nagai M. Int J Mech Sci 1984;26:437.
[54] Petryk H. Arch Comp Meth Engng 1997;4:111.
[55] Chen WH. Int J Solids Structures 1971;7:685.

[56] McMeeking RM, Rice JR. Int J Solids Structures 1975;11:601.
[57] Norris Jr. DM, Moran B, Scudder JK, Quinones DF. J Mech Phys Solids 1978;26:1.
[58] Tvergaard V, Needleman A, Lo KK. J Mech Phys Solids 1981;29:115.
[59] Chen LG. Int J Mech Sci 1983;25:47.
[60] Zbib HM, Jubran JS. Int J Plasticity 1992;8:619.
[61] Tvergaard V. Com Meth Appl Mech Eng 1993;103:273.
[62] Goldthorpe BD, Church P. J Phys IV France 1997;Colloque C3:C3–753.
[63] Hill R. J Mech Phys Solids 1962;10:1.
[64] Rudnicki JW, Rice JR. J Mech Phys Solids 1975;23:371.
[65] Birnbaum HK. Scr Metall 1994;31:149.
[66] Peisl H. In: Alefeld G, Volkl J, editors. Hydrogen in metals I: Topics in applied physics. Springer-Verlag; 1978. p. 28.
[67] Oriani RA. Acta Metall 1970;18:147.
[68] Hirth JP, Carnahan B. Acta Metall 1978;26:1795.
[69] Fuentes-Samaniego R, Gasca-Neri R, Hirth JP. Phil Mag A 1984;49:31.
[70] Taha A, Sofronis P. Eng Fracture Mech 2001;68:803.
[71] Matsui H, Kimura H, Moriya S. Mat Sci Engng 1979;40:207.
[72] Matsui H, Kimura H, Kimura A. Mat Sci Engng 1979;40:227.
[73] Moriya S, Matsui H, Kimura H. Mat Sci Engng 1979;40:217.
[74] Eastman J, Heubaum N, Matsumoto T, Birnbaum HK. Acta Metall 1982;30:1579.
[75] Teter DF, Robertson IM, Birnbaum HK. Acta Mater 2001;49:4313.
[76] Windle AH, Smith GC. Metal Sci Journal 1970;4:136.
[77] Asano S, Otsuka R. Scr Metall 1976;10:1015.
[78] Ulmer DG, Altstetter CJ. Acta Metall 1991;39:1237.
[79] Abraham DP, Altstetter CJ. Metall Trans A 1995;26:2849.
[80] Perrin G, Leblond JB. J Appl Mech 1993;60:842.
[81] Thomas G J. In: Thompson AW, Bernstein IM, editors. Hydrogen effects in metals. Trans Met. Soc. AIME; 1980, p. 77.
[82] Tien JK, Bernstein IM, Richards RJ. Metall Trans A 1976;7:821.
[83] McLellan RB. Acta Metall 1979;27:1655.
[84] Gilman JJ. Micromechanics of flow in solids. McGraw-Hill, 1969 p. 185.
[85] Baker C, Birnbaum HK. Scr Metall 1972;6:851.
[86] Birnbaum, H. K., Private communication.
[87] Lassila DH, Birnbaum HK. Acta Metall 1986;34:1237.
[88] Lassila DH, Birnbaum HK. Acta Metall 1987;35:1815.
[89] Lassila DH, Birnbaum HK. Acta Metall 1988;36:2821.
[90] Zerilli FJ, Armstrong RW. J Appl Phys 1987;61:1816.
[91] Bammann DJ. Mat Sci Engng A 2001;309-310:406.
[92] Ghosh AK. In: Koistinen DP, Wang N-M, editors. Mechanics of sheet metal forming. New York: Plenum Press; 1978. p. 287.
[93] Hutchinson JW, Neale KW. Acta Metall 1977;25:839.
[94] Hutchinson JW, Neale KW. In: Koistinen DP, Wang N-M, editors. Mechanics of sheet metal forming. New York: Plenum Press; 1978. p. 269.
[95] Ghosh AK. J Eng Mater Tech 1977;102:264.
[96] Needleman A, Tvergaard VI. In: Carlsson J, Ohlson NG, editors. Mechanical behavior of materials-IV, Vol. 1. Oxford: Pergamon Press; 1984. p. 51.
[97] Needleman A. Revue Phys Appl 1988;23:585.
[98] Tvergaard V. In: Nguyen QS, editor. Bifurcation and stability of dissipative systems. ICMS No 237. New York: Springer Verlag; 1993. p. 251.
[99] Peirce D, Asaro RJ, Needleman A. Acta Metall 1983;31:1951.